# Chemostratigraphic analysis as a powerful tool for the lateral continuity of structurally complex reservoirs. A case study.

*Liborius-Parada Andreina[1*], Medina-Macedo Marlen[1*], Tonner Dave[1], Hughes Simon[2,] and McCulley Meri[2]*

[1,2] Diversified Well Logging LLC, 9780 Pozos Ln. Conroe Texas 77303, United States.
[1] Pemex Exploración y Producción - Subdirección de Proyectos de Explotación Estratégicos, Avenida Adolfo Ruíz Cortines, Edificio Pirámide, No. 1202, Piso 4, ala B, Fracc. Oropeza Villahermosa, Tabasco, C.P. 86030, México.

**Abstract.**

The Upper Jurassic Kimmeridgian is one of the most important targets and one of the most significant oil discoveries in the Pilar-Reforma-Akal geological province in Mexico. It is laterally heterogeneous and interpreted to be deposited in a marine inner ramp of dark gray oolitic, pelletal, and bioclastic limestone, mostly dolomitized, with anhydrite and shale beds and much dark brown and gray shale. The southern region of the Pilar-Reforma-Akal geological province displays a diverse scale of geological structures that affects the understanding of the lateral extension. The structural complexity can be associated with body salt intrusions, shale diapirism, and listric faults. Preliminary results have shown that the complex modeling workflow obtained by seismic data affected the velocity models, increasing the uncertainty and misinterpreting the depositional environment, formation tops, and lateral continuity. This work aims to establish the reservoir continuity of well G to understand the compositional variation of the Jurassic Kimmeridgian target to investigate relationships between the production intervals and their association with offset wells. This study utilizes a portable, energy-dispersive X-ray fluorescence (ED-XRF) spectrometer for 1156 cutting samples within 4 vertical wells targeting the Jurassic Kimmeridgian in the "X" field. The cuttings were collected every 3-5 meters, revealing broad trends, in conjunction with an extensive QA /QC process that generated a quantitative stratigraphic control during drilling. The principal elements used in this study to indicate detrital sedimentation are zirconium (Zr), titanium (Ti), silicon (Si), cobalt (Co), lead (Pb), niobium (Nb), aluminum (Al), potassium (K), thorium (Th), and phosphorus (P). The amount of quartz, both biogenic and detrital, is inferred using a Si/Al ratio. Biogenic quartz is inferred when detrital influx cannot account for the amount of quartz observed. Strontium (Sr), calcium (Ca), magnesium (Mg), and manganese (Mn) are elements associated with carbonate proxies, and nickel (Ni), copper (Cu), zinc (Zn), uranium (U), molybdenum (Mo), vanadium (V), and sulfur (S) are indicators of basin restriction and associated with paleo-redox/anoxic environments. With the dense database obtained from the offset wells (Well A, B, and I) 3 chemostratigraphic packages and 9 chemofacies were determined for the field of study; the Upper Cretaceous and Middle Cretaceous were characterized by high concentrations of carbonate and detrital proxies, mainly associated with shaley intervals, biogenic quartz, and an increase in the anoxic proxies with a reasonably high pseudo-TOC model, typical of an epicontinental sea. At the same time, the Lower Cretaceous indicated a marked variation of detrital, anoxic proxies with a lower pseudo-TOC. The Upper Middle-Lower Tithonian Jurassic was characterized by oscillations in carbonate, detrital, and anoxic proxies with a variable pseudo-TOC model ranging from "good" to "excellent". On the other hand, the Upper Jurassic Kimmeridgian target indicated the highest Mg concentrations and (the) anoxic conditions not seen in any previously studied Upper Jurassic studied. The chemostratigraphic analysis and the stratigraphic control reduced uncertainty and optimized decision-making during the drilling of well G, acting as a powerful tool to understand the lateral continuity of a structurally complex reservoir.

## 1. Introduction

*Chemostratigraphy* is a technique that can be applied to outcrops, cores, or cuttings samples with an equivalent degree of certainty. It generates a visual and quantitative representation, in real-time, processing the element concentration after the analyses are performed on the rig-site while drilling, generating a chemostratigraphic profile and element ratios of the major, trace, and anoxic elements. These profiles can be used to develop stratigraphic frameworks and correlate units through sedimentary basins as complex as those studied in the present field. Compared with petrography, X-ray diffraction, and TOC data, chemostratigraphy through a large number of measured elements provides an important correlation parameter since it allows the recognition of detrital, carbonate, and paleo-redox/paleoenvironmental indicators using inorganic geochemical proxies also referred to as "chemozones" [1].

The use of chemostratigraphy, among other disciplines such as biostratigraphy and petrography, optimizes the integrated geological-operational model, increasing the efficiency of field development and improving the stratigraphic positioning and formation top picks, which have been pre-determined using downhole petrophysical logs.

Based on the association of elements established by Craigie in 2018 [2], the associations used for these interpretations were classified into three main types:

1. Elements associated with detrital proxies and clay content: zirconium (Zr), titanium (Ti)), silicon (Si), cobalt (Co), lead (Pb), niobium (Nb), aluminum (Al), potassium (K), thorium (Th), phosphorus (P)

* Corresponding author: andreinaliborius@dwl-usa.com

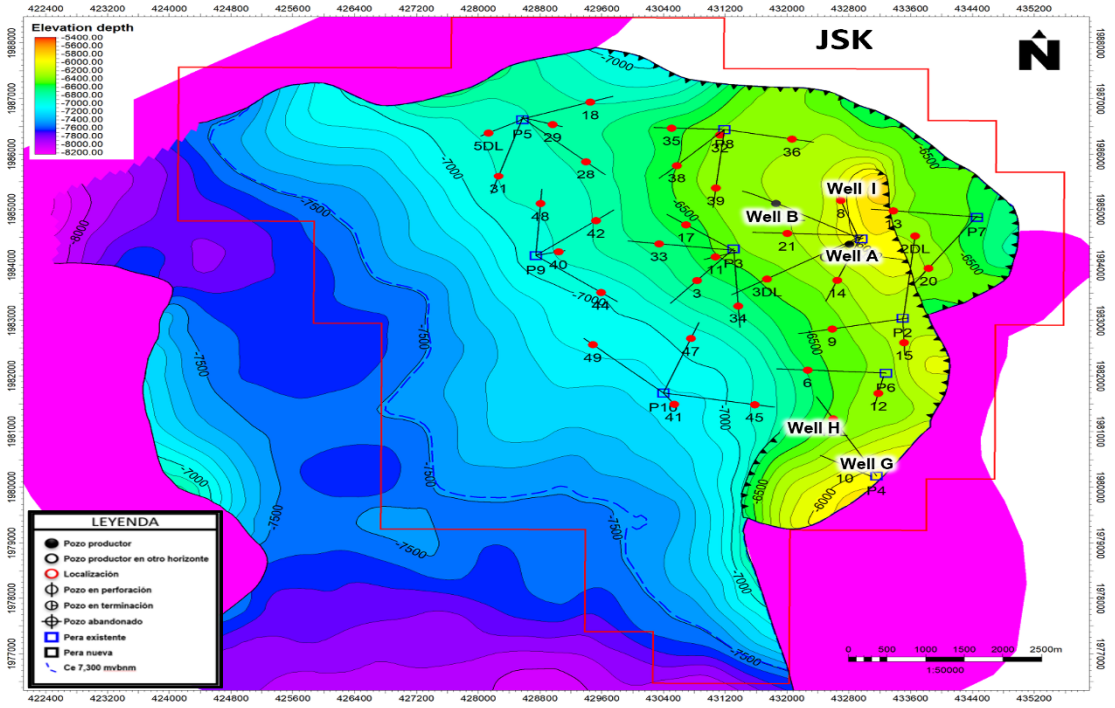


**Fig. 1.** Structural map of the field of study. From D.R. Petroleos Mexicanos, 2021

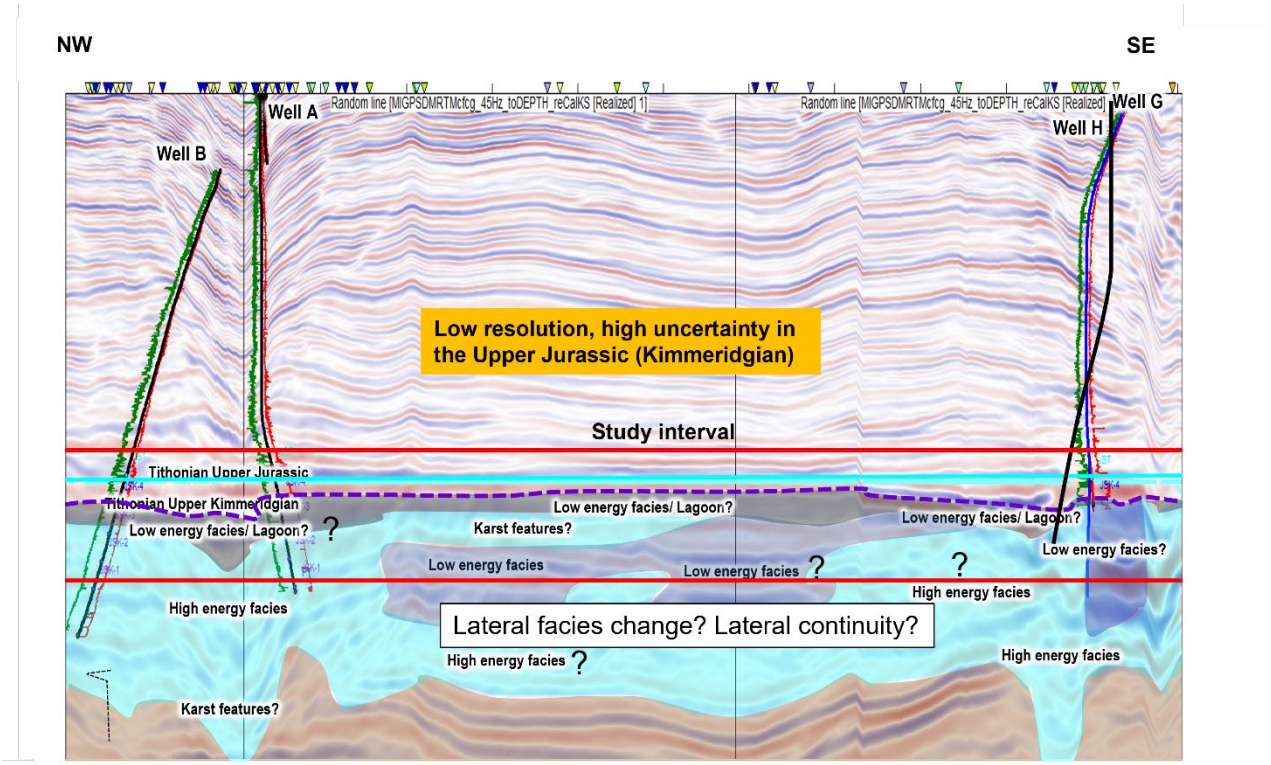


**Fig. 2.** Seismic profile of the study area where the structural complexity is reflected due to the karstic and saline depositional environment. From D.R. Petroleos Mexicanos, 2021.

2. Elements associated with carbonate proxies: strontium (Sr), calcium (Ca), magnesium (Mg), manganese (Mn)
3. Elements associated with paleo-redox / anoxic proxies: nickel (Ni), copper (Cu), zinc (Zn), uranium (U), molybdenum (Mo), vanadium (V), and sulfur (S)

The field of study is characterized by an asymmetric anticline with preferential direction NW-SE with a 3-way closure against saline and reverse faults (Figure 1), where there is a high degree of uncertainty due to the structural complexity and low seismic resolution generated by the salt bodies present in the geological structure (Figure 2). The reservoir's sedimentary model and the environment of deposition correspond to an internal ramp consisting of dolomitized carbonate rocks presenting the development of oolitic banks (Figure 3). The complex stratigraphic settings, together with a high degree of diagenetic alteration, generated significant dolomitic intervals that modify the lateral continuity developing new facies towards the SW. The application of chemostratigraphy, when integrated with other datasets, aided in identifying ideal acreage positions and defining well target zones with the highest reservoir quality.

## 2. Methodology

The methodology performed for chemostratigraphic analyses was based on the collection and integration of cuttings samples from offset wells for a subsequent preliminary interpretation of their chemo-facies. ~10 gr of the sample is washed, rinsed with water in a sieve, and dried at ~40 Celsius. ~5g of sample is ground into a powder in a mechanical mill, and XRF analyses is performed on the powder.

Samples are placed in the upper sieve (mesh # 8), with the mesh #120 sieve under it. In some instances where exceptionally heavy sludge (more than 13ppg) is used, it may be necessary to use an ultrasonic cleaner to loosen and remove stubborn contamination and Barite from the sample. The main reason for the rigorous sample cleaning process before XRF analysis is to remove contamination from samples, that may have been introduced by the

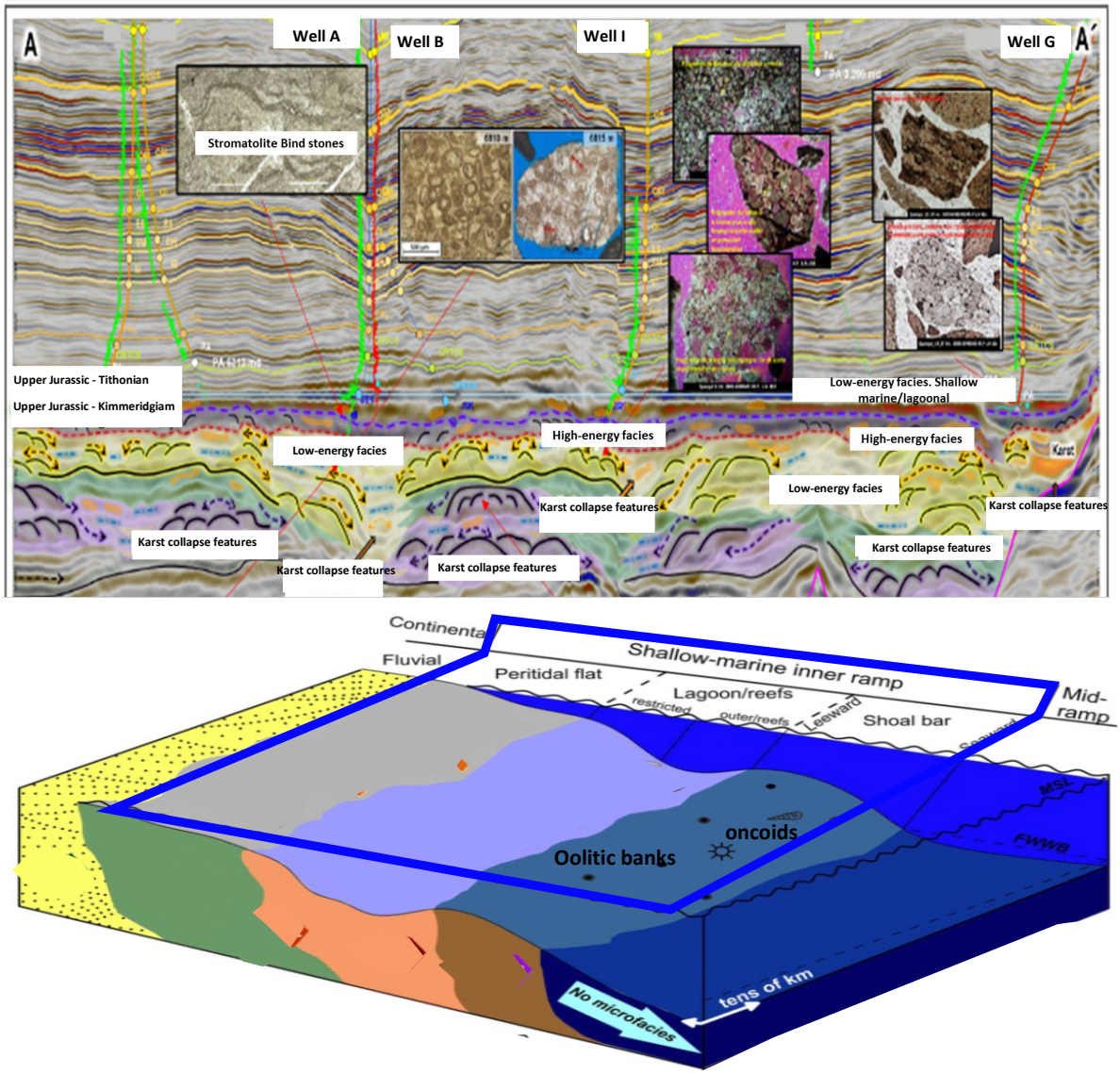


**Fig. 3.** Sedimentary model and lateral facies distribution. From D.R. Petroleos Mexicanos, 2021

sludge system, well structure, platform systems, or other

sources. Contaminants will significantly affect the quality and reliability of the data we provide to the customer, and effective and thorough cleaning is essential to provide quality data.

Complete drying of the sample is essential for accurate analysis and reliable and continuous operation of the XRF machine. If moisture or liquid is present in any amount of sample material, it will instantly convert to steam when the vacuum is applied to the sample chamber, causing internal contamination in the sample chamber. This will have a substantial adverse effect on the data and, over time, will cause contamination to accumulate on the tube and X-ray detector surface, further degrading the data's quality and the machine's longevity. For this reason, the preferred method of drying is by heat.

Lastly, samples are pulverized to start the analysis process. It is necessary to grind the XRF samples into a fine powder to homogenize (mix thoroughly) the sample to ensure that the machine analyzes the full range of forming material in the sample.

X-ray Fluorescence (XRF) analyses is carried out in a portable, energy-dispersive X-ray fluorescence (ED-XRF) spectrometer in conjunction with an extensive QA/QC process which ensures legitimate sample representation, not impacted by any contamination processes, thus providing a quantitative stratigraphic control during drilling.

Stratigraphic chemo and biostratigraphic controls are generated to determine the formation tops and the associated chemofacies. Once the samples have been processed, they are analyzed and integrated, incorporating other data sources with information from different wireline tools, among other disciplines (petrography, petrophysics, 3D seismic interpretation). Each step is explained in detail below.

A. QA/QC process (Quality assurance/quality control every five samples).

One of the most important and determining characteristics is correct geological evaluation and stratigraphic control. This is achieved through the evaluation of major and trace elements relationships.

To obtain accurate values and validate the variations and interpretations, these element analyses must undergo strict quality control. Each element is calibrated based on standards from the United States Geological Survey (USGS). This ensures that the sample measurements have not been affected by contamination by sludge, barium, or other agents that can modify the elemental concentrations.

B. Generation of a chemo-stratigraphic database of the well in sequence:

With the large database obtained from the offset wells (Well A, B, and I) 3 chemostratigraphic packages and 9 chemofacies were determined for the field of study, making it possible to reduce the uncertainty in the determination of the geological column in real-time during the drilling of the study well (Well G).

This methodology applies to all project wells and fields with geological complexity. This technique is of vital importance when the biostratigraphy information is scarce or non-existent, seismic resolution is poor, and the area to be studied is complex. Chemostratigraphic correlations indicate position in the geological column and serve as a reference to indicate fault zones and denote the changes in the paleoenvironment.

C. Elemental Gamma Ray (EGR).

Gamma radiation emitted by elements such as K, Th, and U and their decay products (also called ground-based radiation) exists at trace levels in all subsoil formations. It represents the primary external source of irradiation. Based on this principle, we can offer field records with mineralogy, lithology, and elementary gamma rays based on gamma radiation emitted by uranium, thorium, and potassium (U + Th + K), guaranteeing the quality of the sampling.

This data is beneficial (since it allows an elementary GR record in API units), especially when the LWD tools fail, avoiding the need to rerun tools leading to Non-productive Time (NPT). The higher the sampling density in the well, the greater the utility of the tool as it approaches the depth resolution of a GR Logging While Drilling (LWD) log.

D. Oxides and major elements.

Oxides of major elements are those that predominate in rock chemistry analyses. Among the elements measured in these analyses are Si, Ti, Al, Fe, Mn, Mg, Ca, Na, K, and P, and their concentrations are expressed in the percentage (% wt.) of the oxide. Through a proprietary stoichiometric model developed by Diversified Well Logging, mineralogical modeling was generated from X-ray fluorescence, which contains the most important minerals when performing real-time mineralogical correlations and at the regional level. The elements obtained from the mineralogical model are the following: Quartz, Clay (Illite, Chlorite, Kaolinite), Calcite, Dolomite, Apatite, and Halite.

E. Trace elements or oligo-elements

Trace element analysis can provide critical information for improving geological and oil system models by providing substitutes for paleo-depositional and redox environments. In geochemistry, a trace element is one whose concentration is less than 1000 ppm or 0.1% of the composition of a rock. This suite of elements mainly helps proxies.

F. Paleoredox Indicators.

Understanding the depositional configuration of organically rich sediments in the geological record is crucial to reconstructing the paleoclimate of sedimentary basins and the occurrence of oil source rocks [3,4,5,6]. When organic geochemical analyses are unavailable, the elemental paleoredox proxies (U, Mo, V, P2O5, Cu, Ni, Zn) are typically helpful in evaluating the chemical conditions of old water bodies, degree of oxygenation, salinity, and stratification of the water column in fine-grained sediments. Previous studies had strongly supported that Ni is a clear indicator of the organic sinking

flux, explained by the occurrence of diatoms, which dominate productivity in these systems [7,8,9]; Ni tends to be more soluble under oxidizing conditions and less soluble under reducing conditions. This particularity confers Ni as an excellent element to associate with organic matter concentration. By a linear correlation generated with the Total Organic Content of the pilot well, a proprietary pseudo-TOC model developed by Diversified Well Logging was generated for this study**.**

G. Plots-Binary Geochemical Correlations.

Through different elementary relationships, the correlation of binary plots provided an important degree of correlation ranging from 85-98% accuracy in defining the chemo-stratigraphic units used to correlate the offset wells with the I and G wells.

H. Potential types of clay generated from the binary plot of Potassium and Thorium.

Based on the high concentrations of potassium and thorium in the clays and through the stoichiometric calibration of $K_2O$, a preliminary clay model can be generated from this binary plot. This plot has been very helpful in estimating expansive clays that may affect well conditions or in the geological characterization of anoxic intervals with a high rate of organic matter.

## 3. Chemostratigraphic interpretations and their association with the geological periods

Micropaleontological and petrographic analyses were compared with the chemostratigraphic data, and the ratios of $Ni/Al_2O_3$, $SiO2/Al_2O_3$, $Th/K_2O$, $MgO/Fe_2O_3$, CaO/Sr, and $Al_2O_3/Zr$ and net intensities were found to be the most informative and discriminant. Binary plots correlated each geological period with its specific chemostratigraphic association, decreasing the geological column's uncertainty when drilling.

I. Cretaceous

Chemostratigraphic Package 1 (Units 1.1, 1.2, 1.3, and 1.4) mainly comprises the Upper, Middle, and Lower Cretaceous (Figure 4). The Upper Cretaceous (unit 1.1, 1.2) was characterized by a marked increase of the

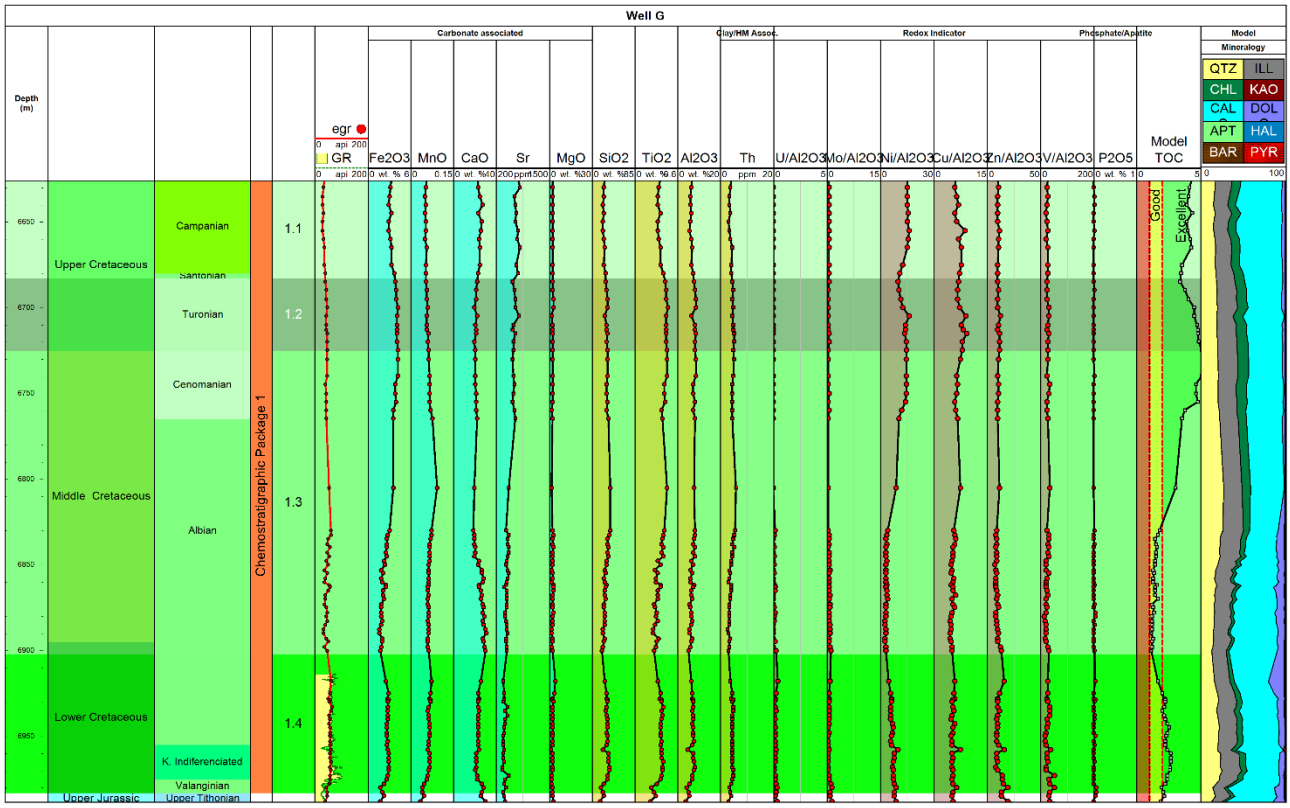


**Fig.4.** Chemostratigraphic profile of majors, trace elements, and paleoredox proxies from the Upper, Middle and Lower Cretaceous

carbonate proxies with 25 wt.% Ca, and low concentrations of Mg and Mn at 2.7 and 0.06 wt.% and 780 ppm Sr on average, respectively. Detrital proxies

displayed a noticeable increase with 29 wt.% Si, 9 wt.% Al, 0.45 wt.% Ti, 2.3 wt.% K, 2.9 wt.% Fe on average.

The mineralogical model generated from the elemental data denotes a high presence of calcite with low concentrations of magnesium, possibly generated from secondary diagenetic processes, and moderate concentrations of quartz, illite, and chlorite associated with shaley intervals. Given the carbonate nature of this sequence, uranium concentrations are typically low. Anoxic proxies remain high throughout the whole interval (179 ppm V, 27 ppm Ni, 39 ppm Cu, and 66 ppm Zn) with a reasonably high pseudo-TOC model. In the Middle Cretaceous (unit 1.3), especially at 6765m-6835m, similar

concentrations for carbonate and detrital proxies remained constant throughout the interval (Carbonate proxies displayed 30 wt.% Ca, 1.97 wt.% Mg, 0.06 wt.% Mn and 450 ppm Sr, and detrital proxies, indicated 25 wt.% Si, 8 wt.% Al, 0.35 wt.% Ti, 2.01 wt.% K, 2 wt.% Fe on average). The anoxic proxies and the pseudo-TOC model remained moderate-high (with 170 ppm V, 29 ppm Ni, 30 ppm Cu, and 63 ppm Zn, on average). As calcium levels reduced at 22 wt.%, uranium concentrations moderately increased at 0.77 ppm. After 6835m, the detrital proxies progressively declined (at 34 wt.% Si, 9 wt.% Al, 0.40 wt.% Ti, 2.5 wt.% K, 3.1 wt.% Fe on average). In contrast, the carbonate proxies notably increased (32 wt.% Ca, 4.65 wt.% Mg, 0.07wt.% Mn, and 525 ppm Sr, on average), going for an elemental and lithological transition from homogeneous (marly) claystone to increasingly $CaCO_3$-rich marls and limestones. Anoxic proxies decrease simultaneously (with 156 ppm V, 26 ppm Ni, 25 ppm Cu, and 50 ppm Zn, on average), and the pseudo-TOC model declines significantly.

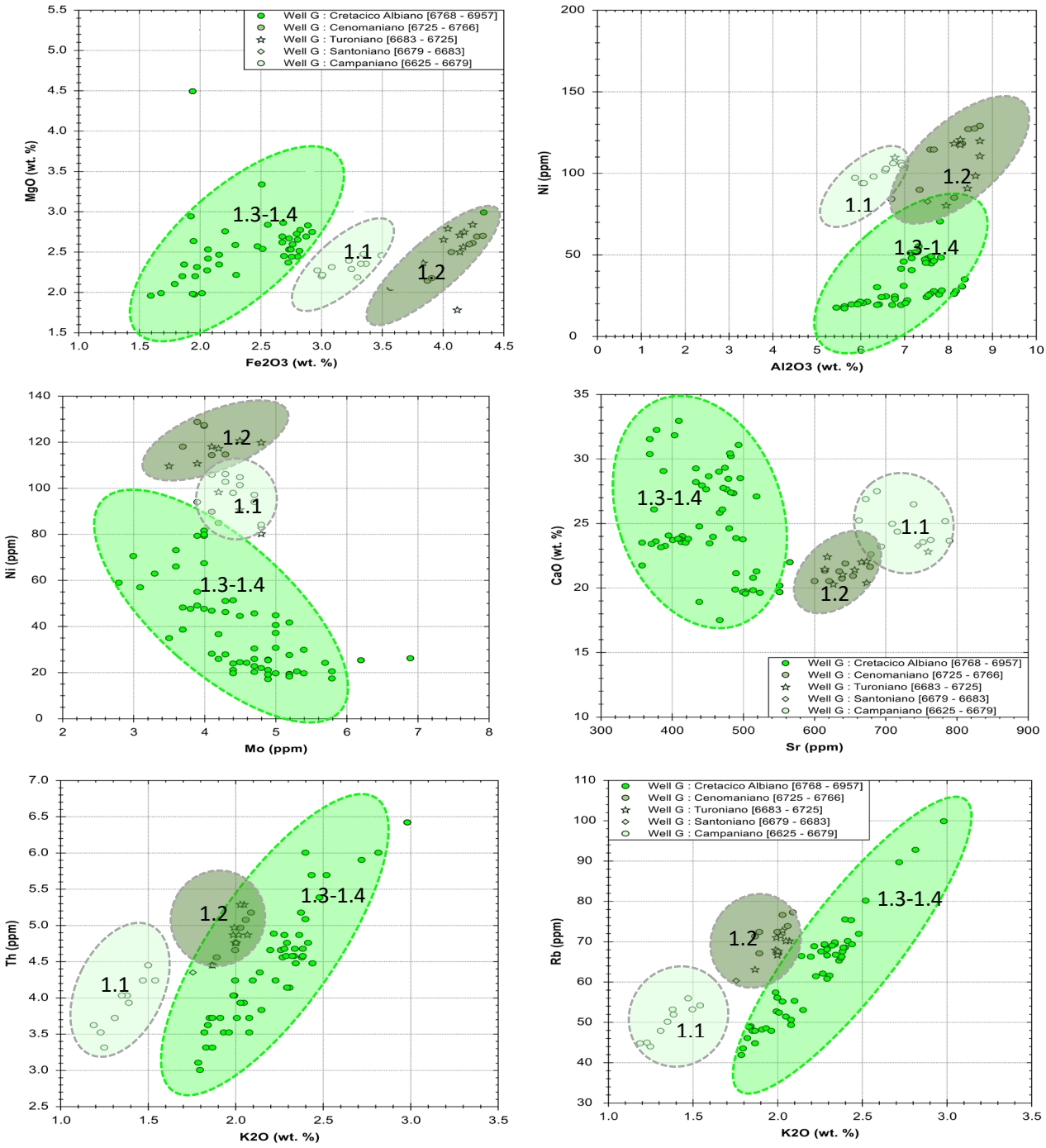


**Fig. 5.** Discrimination of chemostratigraphic units 1.1 and 1.2. Binary plots and association of chemo-facies in the Cretaceous (Albian, Cenomanian, Turonian, Santonian, and Campanian). A dashed bright green circle is associated with the Albian; a dashed olive-grey circle to the Cenomanian-Santonian, and a light green dashed circle to the Campanian

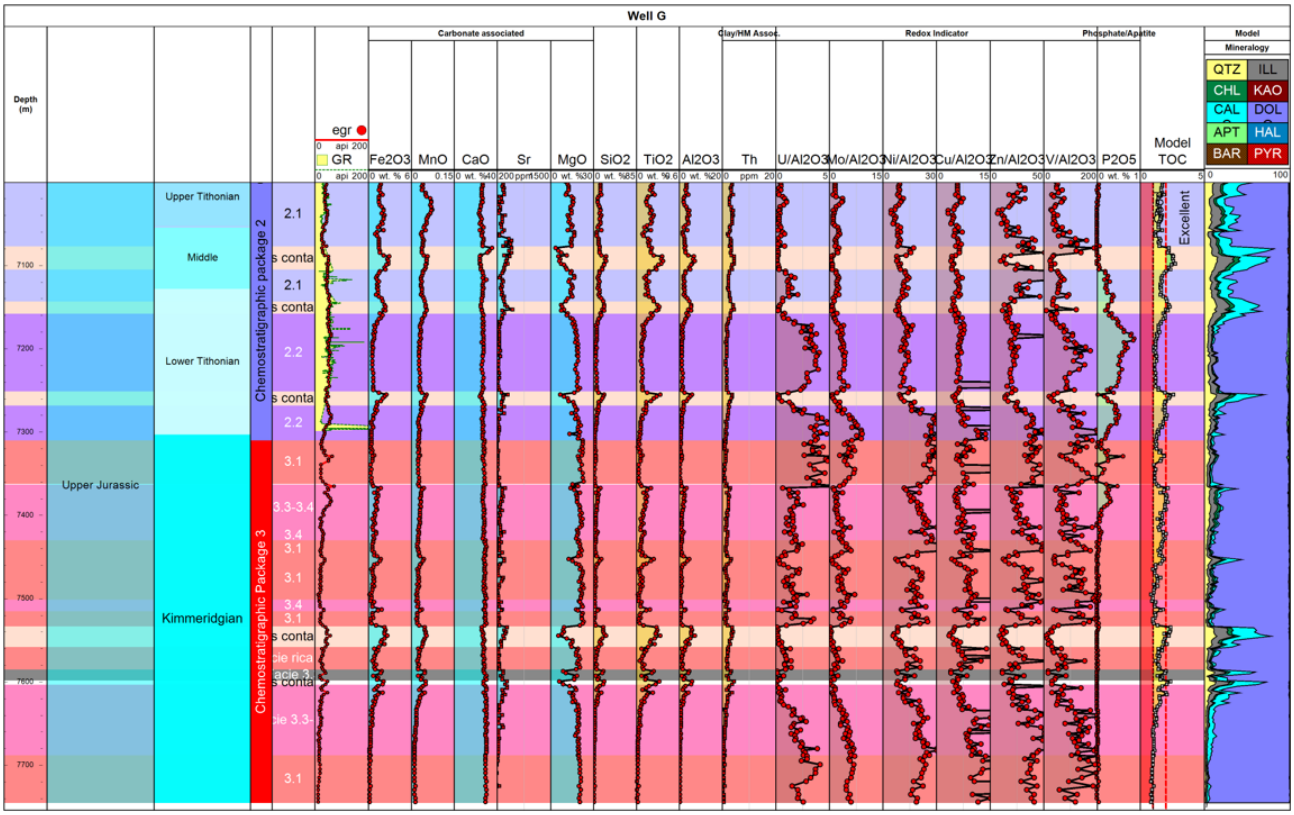


**Fig. 6.** Chemostratigraphic profile of majors, trace elements, and paleoredox proxies from the Upper Jurassic

Biostratigraphic data was absent in the Lower Cretaceous, at depths 6925m-6977m. However, the high sample density obtained from previous wells developed a chemostratigraphic correlation by the use of binary plots in Figure 5 ($MgO/Fe_2O_3$; Ni/Al; Ni/Mo; CaO/Sr; $Th/K_2O$ and $Rb/K_2O$) that allowed to correlate the biologically barren interval with the 1.1 unit. The present correlation displays one of the most important correlations when we no longer can rely on biostratigraphic data.

Furthermore, in the Lower Cretaceous, at depths 6902m-6926m, a marked increase in the carbonate and paleoredox proxies (carbonate proxies at 34 wt.% Ca, 4.7 wt.% Mg, 0.09wt.% Mn, and 630 ppm Sr and paleoredox proxies at 280 ppm V, 47 ppm Ni, 40 ppm Cu, and 103 ppm Zn and 2.53 ppm U on average) displayed a new chemostratigraphic unit markedly differs from the previous units.

This horizon was named the chemostratigraphic unit 1.4. From the sequence-stratigraphic point of view, unit 1.4 could be associated with a maximum flooding surface often seen in the Albian in equivalent formations worldwide, where high paleoredox proxies displayed exceptionally high U, V, Cu, Mo, Zn, and Ni enrichments, representing environments associated with low oxygen concentrations.

## II. Jurassic

It is known worldwide that in the Upper Jurassic, the Tithonian dolomite-rich beds were predominantly confined to the mound facies; The initial massive matrix dolomitization can be related to pressure dissolution during a very shallow burial, at temperatures of at least 50°C, where burial compaction provided sufficient fluids for dolomitization [10]. For well G, the Upper Jurassic Tithonian at a depth interval of 6990m-7303m was characterized by a noted reduction of detrital proxies (6 wt.% Si, 1.4 wt.% Al, 0.09 wt.% Ti, 0.53 wt.% K, 0.72 wt.% Fe on average) and a marked increase of the carbonate proxies (32 wt.% Ca, 19 wt.% Mg, 0.03 wt.% Mn, and 263ppm Sr on average ), where magnesium concentrations remained constant throughout the whole interval. Despite the importance of magnesium in the early Upper Jurassic, calcium concentrations can be found as high as 20-23 wt. %.

From base to top, anoxic proxies represented a significant increase in V, Ni, Cu, Mo, and Zn (at 260 ppm; 240 ppm; 5 ppm, and 50 ppm, respectively) with a marked increase in phosphorus of 0.87 wt.% at the end of the Lower Tithonian, which according to some authors [11], represents an increase in phosphorus accumulation rate from microfauna, coincided with the worldwide Nannofossil Calcification Event, related to a bloom of strongly calcified calcareous nannoplankton taxa. The mineralogical model displayed a noticeable presence of dolomite with fewer calcite, illite, chlorite, and quartz

percentages. The pseudo-TOC model remained steady and is categorized as "good." This interval is associated with the chemostratigraphic package 2, units 2.1 and 2.2.

While analyzing samples in real-time at the rigg-site, we came across intervals that, according to the previously mentioned binary plots association, denoted the presence of unit 1.1, along with highly contaminated barium

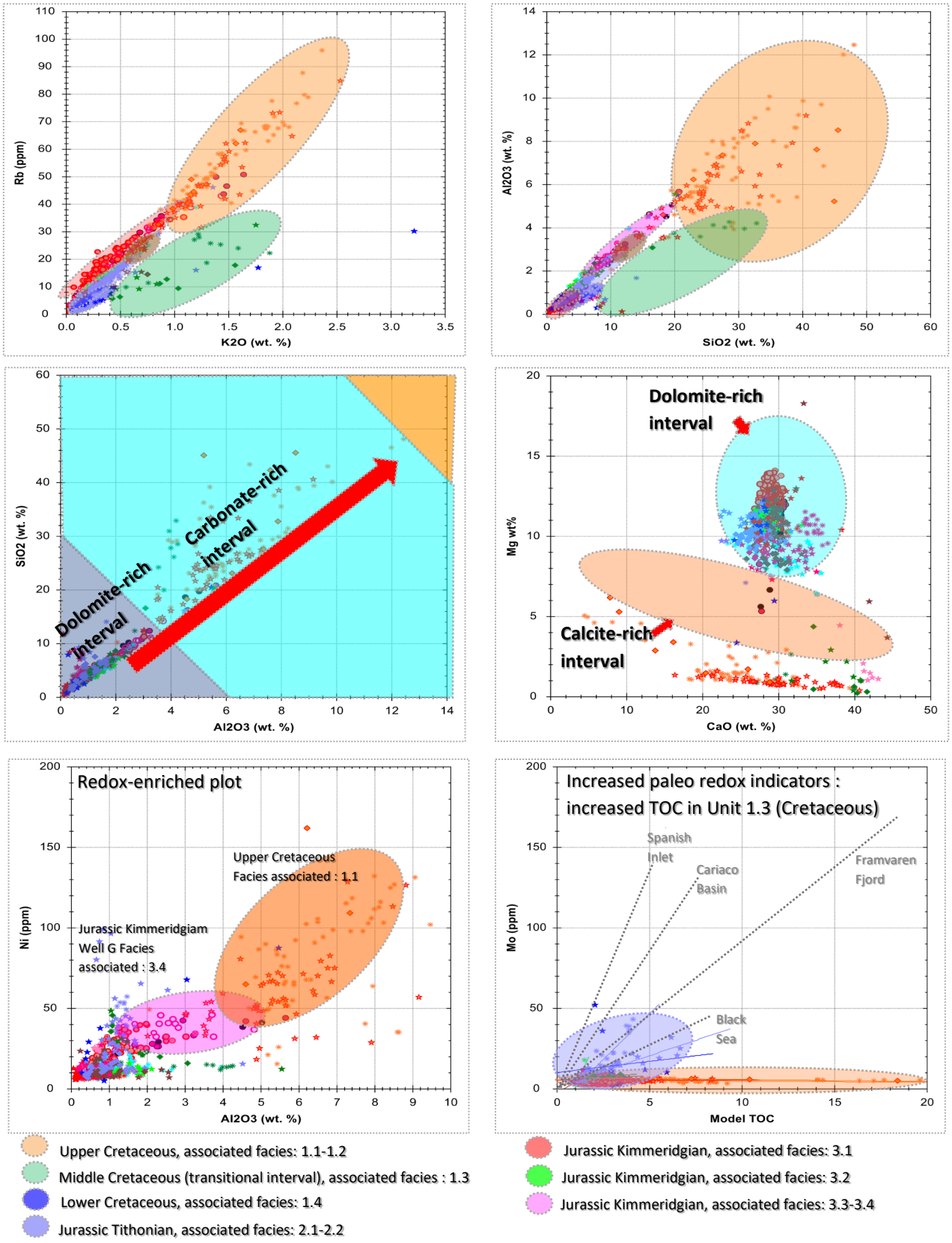


**Fig. 7.** Discrimination of chemostratigraphic units in the Cretaceous and the Jurassic period. Binary plots (Ni (ppm) vs. $Al_2O_3$ (wt.%); $SiO_2$ (wt.%) vs. $Al_2O_3$ (wt.%); Rb vs. $K_2O$ and Mo (ppm) vs. the pseudo-TOC model) and association of chemo-facies to the geological period. The light-orange circle is associated with Upper Cretaceous (Unit 1.1-1.2), Dark-green with Middle Cretaceous (Unit 1.3) ; Blue with Lower Cretaceous (Unit 1.4); Light-purple with Jurassic Tithonian (Unit 2.1-2.2); Light-red with Jurassic Kimmerdgian (Unit 3.1); Light-green with Jurassic Kimmeridgian (Unit 3.1, 3.2 and 3.3) and light-pink with Jurassic Kimmeridgian (Unit 3.4).

intervals where it was expected to see the Upper Jurassic samples. Based on the data obtained from chemostratigraphy and the reported biostratigraphy, it was interesting to notice that each time the well resumed operations, cuttings from above were contaminating the first interval samples, not displaying an accurate representation of the data.

This example can highlight the importance of real-time chemostratigraphy to differentiate contaminated intervals from variations in the depositional environment properly. In addition, chemostratigraphic sampling can provide important operational information to improve hole cleaning and wellbore stability. Furthermore, the Upper Jurassic Kimmeridgian (Figure 6) indicated the highest magnesium-rich interval, not previously seen in any of the wells previously studied in the field.

As mentioned before, specific proxies and binary relationships such as Ni (ppm) vs. $Al_2O_3$ (wt.%); $SiO_2$ (wt.%) Vs. $Al_2O_3$ (wt.%); Th vs. $K_2O$; Rb vs. $K_2O$ and Mo (ppm) vs. the pseudo-TOC model allowed the understanding of the paleoenvironmental conditions for the Lower and Upper Cretaceous and Upper Jurassic (Figure 7).

When compared with the Upper Jurassic, a noticeable enrichment in the paleoredox proxies' concentrations was observed for the Upper Cretaceous; The anoxic proxies reduced, becoming more oxidizing (decreased concentrations in the paleoredox proxies at 128 ppm V, 34 ppm Ni, 11 ppm Cu, and 45 ppm Zn and 1.50 ppm U on average) generating a new chemostratigraphic package 3 (units 3.1, 3.3 and 3.4). However, the G well behaved slightly differently from the previous wells in the field since it displayed a lateral variation of chemo-facies with higher Mg, Al, Fe, and Zr concentrations as well as an increase of the paleoredox proxies such as U, Mo, V, $P_2O5$, Cu, Ni, and Zn.

From the chemostratigraphic point of view, it could be predicted that the G well might display a much more favorable environment of deposition prone to developing good preservation of organic matter. Furthermore, it is also believed that the structural complexity could also affect the oil window, generating a better prospectivity than the previously analyzed nearby wells.

Figure 8 shows a structural section that displays the integration of geological data generated by the chemostratigraphy and biostratigraphy interpretation. Undoubtedly, the synergy of the two disciplines determined a better stratigraphic correlation for the structurally complex field of study.

Uncertainty was reduced when the formation tops were quantitatively picked, developing an accurate geological column in real-time, which showed an increase in thickness towards the southeast for the Upper Tithonian and Kimmeridgian interval, perhaps associated with the karstic and subsalt structural control that potentially affected the thickness and even the diagenesis of the latest deposits.

**Conclusions**

Chemostratigraphic analyses, in conjunction with the ages provided by biostratigraphy, generated stratigraphic control while drilling, reducing the uncertainty and optimized decision-making during the wellbore completion process.

Chemostratigraphic interpretations are augmented through a comprehensive understanding of the mineralogical relationships between the elements and the regional geology.

The methodology generated by the QA/QC control and the elaboration of a mineralogical model from the elemental data recognizes subtle changes in the depositional environment that a standard set of records or even a visual inspection cannot detect.

A noticeable enrichment of paleoredox proxies was observed for the Upper Cretaceous in G well, where the paleoredox proxies associated with elements such as U, Mo, V, $P_2O5$, Cu, Ni, and Zn displayed an increase in the redox conditions and a lateral variation of chemo-facies more favorable environment of deposition, prone to developing good preservation of organic matter for well G.

Furthermore, according to seismic data, the structural complexity found in the study area (salt intrusions, shale diapirism, and listric faults) could also affect the oil window, generating a better prospectivity than the nearby wells analyzed. It is important to understand when mineralogical composition and/or organic matter content is lacking while drilling. Chemostratigraphy would reduce the level of uncertainty as a helpful tool for understanding the lateral continuity of a geologically complex area.

Another advantage of using real-time chemostratigraphic interpretations could be attributed to the fauna's absence during the development of the geological column. Certain intervals in the geological column denoted scattered / absent fauna for some of the drilled Upper Jurassic intervals with no age dating for the specific intervals. Chemostratigraphic relationships and binaries plots correlated areas where biostratigraphy was absent, generating a chemostratigraphic association between units that determined lateral chemo-facies changes. An increase in diagenetical processes toward SE and especially for the G-well could be caused by the mechanical and chemical compaction in the sediments' primary textural and mineralogical composition at the deposition time and after

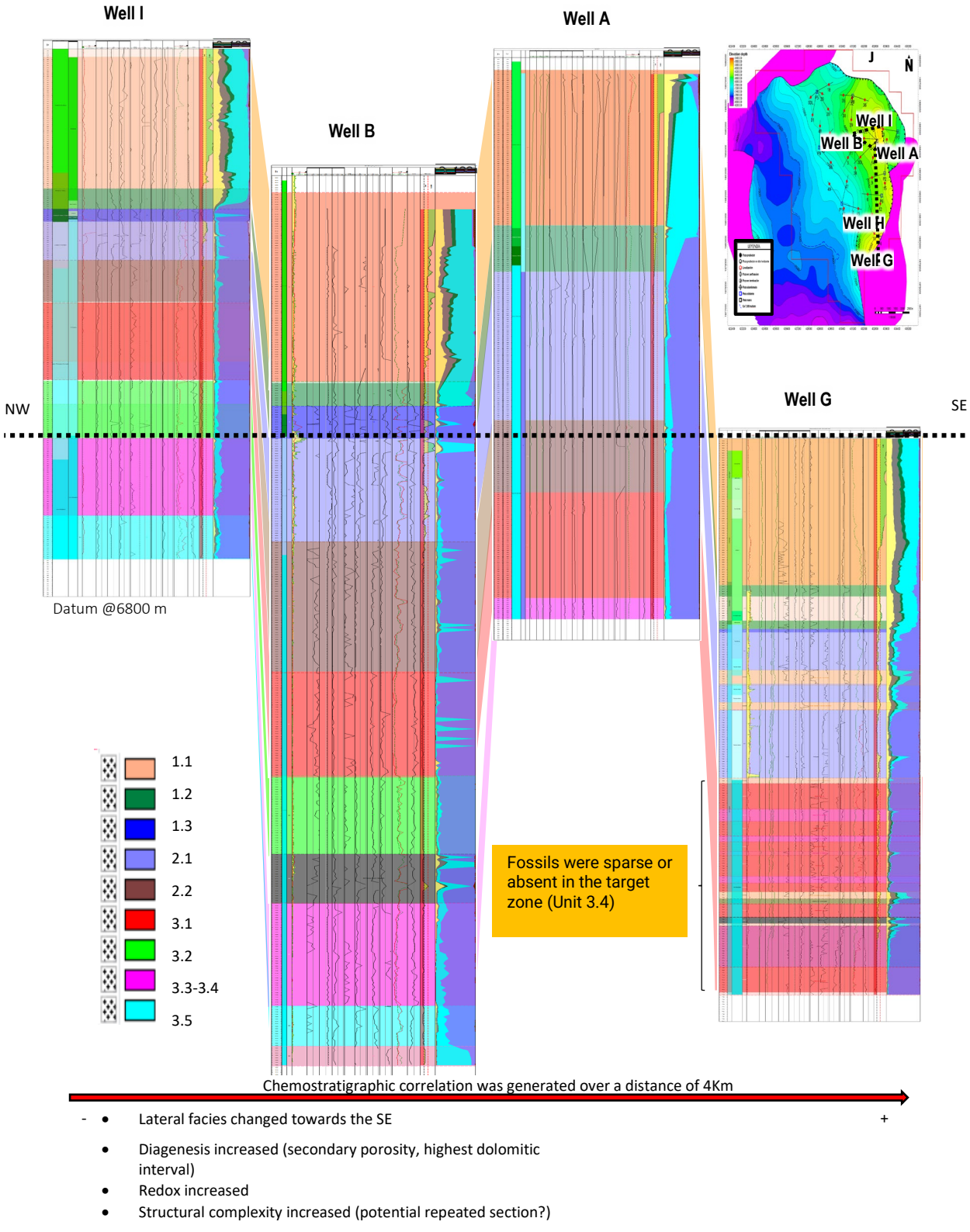


**Fig. 8.** Final chemostratigraphy correlations (per chemostratigraphy unit) for the Cretaceous and Upper Jurassic formations (structural cross-section).

burial diagenesis. Real-time petrographic and lithological analyses have validated these results with higher concentrations of Mg, Al, Fe, and Zr. The increase of the paleoredox proxies (U, Mo, V, $P_2O_5$, Cu, Ni, Zn) and the pseudo-TOC model predict a

In conjunction with micropaleontological and petrographic analyses, real-time chemostratigraphy contributed to successful well completion. It generated a high-level regional stratigraphic correlation, allowing an understanding of the lateral variation and deposition environment using the chemofacies as vertical correlation parameters.

Through the information provided by these analyses in developing a comprehensive stratigraphic framework, it is possible to improve well construction decision-making through greater geological certainty. This has practical applications for geo-stopping, geo-steering, picking casing points, picking coring points, and other real-time decisions.

**Acknowledgments**

Special thanks to the PETRICORE geoteam: Isaac Montes Silva, Miguel Martinez, Alejandro Pumarino, and Dr. Jose Berlanga Garcia. Thank you for the biostratigraphic data to culminate this project.

**References**

1. Ratcliffe, K., Martin, J., Pearce, T., Hughes, A., Lawton, D., & Wray, D. 2006. Regional chemo stratigraphically defined correlation framework for the Late Triassic TAG-I formation in blocks 402 and 405a, Algeria. *Petroleum Geoscience*, *12*(1), 3-12.

2. Craigie, N. 2018. *Principles of Elemental chemostratigraphy: A Practical User Guide.* New York, NY: Springer International Publishing, 189p.

3. Demaison, G. J., & Moore, G. T. 1980. Anoxic environments and oil source bed genesis. *AAPG Bulletin*, *64*(8), 1179-1209

4. Calvert, S. E., Bustin, R. M., & Pedersen, T. F. 1992. Lack of evidence for enhanced preservation of sedimentary organic matter in the oxygen minimum of the Gulf of California. *Geology*, *20*(8), 757-760.

5. Arthur, M. A., & Sageman, B. B. 1994. Marine black shales: depositional mechanisms and environments of ancient deposits. *Annual Review of Earth and Planetary Sciences*, *22*(1), 499-551.

6. Sageman, B. B., Murphy, A. E., Werne, J. P., Ver Straeten, C. A., Hollander, D. J., & Lyons, T. W. 2003. A tale of shales: the relative roles of production, decomposition, and dilution in the accumulation of organic-rich strata, Middle-Upper Devonian, Appalachian basin. *Chemical Geology*, *195*(1-4), 229-273.

7. Böning, P., Shaw, T., Pahnke, K., & Brumsack, H. J. 2015. Nickel is an indicator of fresh organic matter in upwelling sediments. *Geochimica et Cosmochimica Acta*, *162*, 99-108.

8. Lewan, M. D., & Maynard, J. B. 1982. Factors controlling enrichment of vanadium and nickel in the bitumen of organic sedimentary rocks. *Geochimica et Cosmochimica Acta*, *46*(12), 2547-2560.

9. Filby, R. H. 1994. Origin and nature of trace element species in crude oils, bitumens, and kerogens: implications for correlation and other geochemical studies. *Geological Society, London, Special Publications*, *78*(1), 203-219.

10. Reinhold, C. 1998. Multiple episodes of dolomitization and dolomite recrystallization during shallow burial in Upper Jurassic shelf carbonates : eastern Swabian Alb, southern Germany. *Sedimentary Geology*, *121*(1-2), 71-95.

11. Grabowski, J., Haas, J., Stoykova, K., Wierzbowski, H., & Brański, P. (2017). Environmental changes around the Jurassic/Cretaceous transition : New nannofossil, chemostratigraphic, and stable isotope data from the Lókút section (Transdanubian Range, Hungary). *Sedimentary Geology*, *360*, 54-72.